Applied Catalysis B: Environmental 236 (2018) 314–325

Contents lists available at ScienceDirect

Applied Catalysis B: Environmental

journal homepage: www.elsevier.com/locate/apcatb

Exploration of surface properties of Sb-promoted copper vanadate catalysts for selective catalytic reduction of NO_X by NH_3

Jongsik Kim[a,1], Dong Wook Kwon[a], Somin Lee[a,b], Heon Phil Ha[a,c,*]

[a] Materials Architecturing Research Center, Korea Institute of Science and Technology, Seoul, 02792, South Korea
[b] Department of Chemical and Biological Engineering, Korea University, Seoul, 02841, South Korea
[c] Department of Nanomaterials Science and Engineering, University of Science and Technology, Daejeon, 34113, South Korea

ARTICLE INFO

Keywords:
Vanadium oxide
Copper vanadate
Antimony
Selective catalytic reduction of NO_X
NH_3

ABSTRACT

A way to fulfill efficient exploitation of desired catalytic nature provided by V oxide is to modify its chemical structure through the incorporation of secondary transition metal species. This paper reports the use of Cu as a modifier of high-valent V oxide (V_2O_5) to produce a class of copper vanadates and their utilization as active sites for the selective catalytic reduction of NO_X (X = 1 or 2) by NH_3 (NH_3-SCR). All catalysts contained ~2 nm-sized copper vanadate particles highly dispersed on anatase with desired vanadate phases. The anatase-supported $Cu_5V_2O_{10}$ provided a greater quantity of acid sites with improved redox character than $Cu_1V_2O_6$, $Cu_2V_2O_7$, and $Cu_3V_2O_8$, thereby exhibiting the greatest NH_3-SCR performance under ideal reaction conditions. Anatase-supported $Cu_3V_2O_8$, however, was found to possess the most preferred surface properties among the catalysts post sulfation. This was evidenced by NH_3-SCR runs of the catalysts under reaction conditions with H_2O and SO_2-including stream, where all catalysts were pre-sulfated by SO_2 and O_2 at elevated temperatures. The NH_3-SCR performance of the optimum $Cu_3V_2O_8$ on anatase was further promoted after sulfation of the catalyst with the optimum content of Sb promoter. The Sb promoter was verified to enhance the redox feature and minimize the interactions among catalyst surfaces and SO_2/ammonium (bi)sulfates during the NH_3-SCR, as evidenced by durability experiments. While showing N_2 selectivities as ~100% at ≤ 400 °C, the optimized Sb-promoted $Cu_3V_2O_8$ on anatase showed high NO_X conversions (≥ ~85%) at ≥ 220 °C and outperformed the control vanadia-tungstate on anatase, which was used to simulate a commercial catalyst. This paper remarks the exploration of the variable structures of metal vanadates can be a good strategy to discover high-performance catalytic solids for the reduction of NO_X species.

1. Introduction

Vanadium (V) oxides have shown appreciable potential as catalytic solids for various chemical transformations involving the scission/activation of C–H, C–O, N–H, N–O, or C–S bonds [1–3]. This is due to the *multi*-functional surface properties of V oxides to provide great redox character [4,5] and tunable Brönsted or Lewis acidity [6,7], all of which are possible through the alteration of the crystal structures of the V oxides [8–10]. It has been reported that the geometric or electronic features of V_2O_5 (V^{5+}) and VO_2 (V^{4+}) were favorable to provide greater amount of catalytic surface defects than V_2O_3 (V^{3+}) and its low-valent V analogues ($V^{\delta+}$, where $0 < \delta < 3$) [8–10]. Hence, high-valent V oxides (*i.e.*, V_2O_5 and VO_2) often outperformed their counterparts in various redox reactions [8,11–13].

Such examples can be found in the literature reports [8,11–13], among which the selective catalytic reduction of NO_X (X = 1 or 2) by NH_3 to form N_2 and H_2O is recently highly-profiled (denoted as NH_3-SCR in Fig. 1(a)) [14–17]. This recent interest is because of a major side-effect of NO_X, that is, it plays a role as a precursor in the formation of ultra-fine particulate matter, which causes severe air pollution [14–17]. For NH_3-SCR, high-valent V oxides exhibit moderate NO_X conversions and good N_2 selectivities at 300–400 °C [14–17]. This results from two primary roles of the multiple surface sites present in the high-valent V oxides, one of which is to provide Brönsted acid sites ($V^{5+}-OH$) or coordinatively unsaturated Lewis acid sites (V^{5+}) to bind with NH_3 *via* the formation of $V^{5+}-O^-\cdots NH_4^+$ or $V^{5+}\cdots NH_3$ (Fig. 1(b)) [18–21]. The other role of these V oxides has been reported to be the acceleration of NO_X turnover *via* redox cycle. Coordinatively-saturated V^{5+} sites ($V^{5+}=O$) first bind with NO to form $V^{4+}\cdots NO_2$ intermediates and are transformed into $V^{4+}\cdots OH$ upon the generation

* Corresponding author at: Materials Architecturing Research Center, Korea Institute of Science and Technology, Seoul, 02792, South Korea.
E-mail addresses: jkim40@kist.re.kr (J. Kim), dwkwon@kist.re.kr (D.W. Kwon), 217010@kist.re.kr (S. Lee), heonphil@kist.re.kr (H.P. Ha).
[1] 1st author.

https://doi.org/10.1016/j.apcatb.2018.05.024
Received 25 January 2018; Received in revised form 5 May 2018; Accepted 8 May 2018
Available online 15 May 2018
0926-3373/

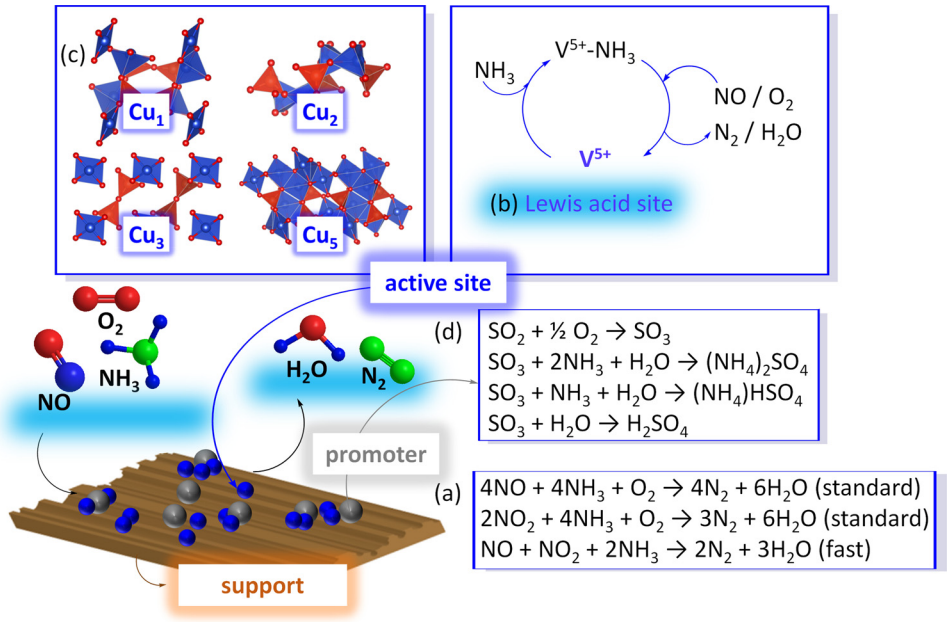

Fig. 1. Schematic representation of selective catalytic reduction of NO_X by NH_3 (NH_3-SCR). Stoichiometry in 'ball-and-stick' is not considered for simplicity. (a) Standard SCR and fast SCR. (b) Surface reaction mechanism on VO_X-based catalytic surface including Lewis acid sites. In (b), reaction stoichiometry is ignored for simplicity. (c) Crystal structures of copper vanadates such as $Cu_1V_2O_6$ (Cu_1), $Cu_2V_2O_7$ (Cu_2), $Cu_3V_2O_8$ (Cu_3), and $Cu_5V_2O_{10}$ (Cu_5). (d) A series of reactions accounting for the generation of ammonium (bi) sulfates (ABS).

of two products (*i.e.*, N_2 and H_2O). This terminates the cycle *via* oxidation, recovering $V^{5+}=O$ while releasing H_2O [18,19,21]. Aforementioned catalytic roles of the surface V^{5+} sites can be further improved when utilizing tungsten oxide (WO_3) and anatase (TiO_2) as a promoter and support, respectively [22,23]. WO_3 helps 1) to suppress the generation of bulk polymeric V aggregates [24] and 2) to retain Brönsted acid sites even at NH_3-SCR temperatures greater than 300 °C [25], whereas catalytic surfaces can accommodate surface-mobile, labile oxygen species to facilitate redox cycle during NH_3-SCR [26,27]. Notably, these benefits could aid in commercializing V_2O_5-WO_3/TiO_2 catalysts for mobile/stationary NO_X emission control units [14–17].

To synthesize a catalyst that outperforms V_2O_5-WO_3/TiO_2 for NH_3-SCR, it is promising to modify V_2O_5 through the incorporation of the secondary metal species (*e.g.*, Ce, Fe, or Mn), leading to the formation of a novel, interesting class of bimetallic V oxides such as $CeVO_4$, $FeVO_4$ and MnV_2O_6 [28–32]. These bimetallic oxides have higher melting points than V_2O_5 and are expected to circumvent the sublimation of toxic V during NH_3-SCR (*i.e.*, 850 °C for $FeVO_4$; 1030 °C for MnV_2O_6; 690 °C for V_2O_5) [33–35]. In conjunction with providing a larger quantity of Brönsted acid sites than V_2O_5, $CeVO_4$ has been reported to 1) stabilize the surface V^{5+} species [28] and 2) accelerate NO_2 production from NO by surface Ce^{4+} species, which could help spur the *so-called* 'fast SCR' (Fig. 1(a)) [28]. In addition, $FeVO_4$ has been shown to incorporate a large quantity of surface defects available to adsorb or activate reactants because of the presence of unique Fe^{3+}-O-V^{5+} linkages [30].

Given the benefits of bimetallic V oxides as catalytic sites for the NH_3-SCR stated above, here we synthesized a series of bimetallic copper vanadate phases active to NH_3-SCR, all of which are well-defined in the CuO-V_2O_5 binary phase diagram such as $Cu_1V_2O_6$, $Cu_2V_2O_7$, $Cu_3V_2O_8$, and $Cu_5V_2O_{10}$ [33,36]. These are denoted as Cu_1, Cu_2, Cu_3, and Cu_5 for simplicity, whereas commercially-available mesoporous anatase (*i.e.*, DT51) was employed as a support to disperse the copper vanadates. Note that an anatase-supported copper vanadate catalyst was previously synthesized for NH_3-SCR by D. Zhang and co-workers [32]. Albeit it showed good NH_3-SCR performance, this catalyst contained mixed bulk phases of CuO, Cu_1, and Cu_2 [32]. Thus, this remains a critical question: 'Which phase among copper vanadate phases does show outstanding NH_3-SCR performance?' This paper details our efforts to answer this question by testing three major hypotheses, which are specified below.

All vanadates crystallize in the *monoclinic* crystal system [33], which allows for the exclusion of different bulk phase-driven geometric effects on the NH_3-SCR performance. Interestingly, Cu_1 consists of distorted octahedral VO_6 sub-units: The V species in Cu_1 are coordinatively saturated by six oxygen atoms and thus are not accessible to NH_3 [33,36]. In contrast, other structures consist of tetrahedral VO_4 sub-units, where the local V environment is open and therefore accessible to NH_3 (Fig. 1(c)) [33,36]. We, therefore, constructed our first hypothesis: 'Cu_2, Cu_3, and Cu_5 can outperform Cu_1 because of the enhanced NH_3 accessibility to the open V^{5+} sites compared to those in Cu_1 during NH_3-SCR.' We also established our second hypothesis such that 'The different atom connectivities of copper vanadates affect the amount of Brönsted acid sites or redox sites present in the resulting catalysts, leading to different NH_3-SCR performance.'

To further promote the NH_3-SCR performance of the catalysts at ≤ 300 °C, the catalysts must be resistant to SO_2 and its derivatives [37–41]. In the course of NH_3-SCR, SO_2 can be oxidized to form SO_3 and sequentially react with NH_3 and H_2O to form ammonium (bi) sulfates (ABS), as illustrated in Fig. 1(d) [37–41]. The ABS species then poison the catalyst surface, limiting the NO_X/NH_3 accessibility during NH_3-SCR [37–41]. This motivated us to use antimony (Sb) as a promoter for the catalysts. Our choice of Sb is based on our previous studies, which have clarified the ability of Sb to reduce the binding energy between catalytic surfaces and SO_2/ABS species [39,41–44]. Our third hypothesis is that 'The NH_3-SCR performance of the catalysts can be maximized by optimizing the Sb composition, where the synergistic effect among copper vanadates and Sb species is predominant.' All catalysts were synthesized, characterized, and tested for the NH_3-SCR to test our three hypotheses. A control, simulating a commercial V_2O_5-WO_3/TiO_2 catalyst, was also synthesized for comparison and tested for NH_3-SCR.

2. Material and methods

2.1. Chemicals

All chemicals were used as-received: $Cu(NO_3)_2{\cdot}3H_2O$ (Daejung, ≥ 99.0%), NH_4VO_3 (Junsei, ≥ 99.0%), $(NH_4)_6H_2W_{12}O_{40}{\cdot}xH_2O$ (Aldrich, 99.99% trace metal basis), $Sb(CH_3COO)_3$ (Alfa Aesar, 97%), DT51 (Cristal Global Co.), $C_2H_2O_4{\cdot}2H_2O$ (Junsei, 99.5–100.2 %), and glacial acetic acid (J. T. Baker, ≥ 99.9%). All gases were purchased from Shinyang: N_2, O_2, Ar, He, 5 vol. % NO/N_2, 5 vol. % NH_3/N_2, 5 vol. % SO_2/N_2, 5 vol. % SO_2/He, 10 vol. % H_2/Ar, 5 vol. % O_2/He, 10 vol. %

O_2/He, 5 vol. % CO/N_2, and liquid N_2.

2.2. Synthesis of anatase-supported copper vanadates

A series of anatase (DT51)-supported copper vanadate catalysts were synthesized according to a procedure detailed elsewhere but with slight modifications [33,34,36]. The catalysts are denoted as Cu_X/DT51, where X = 1 for $Cu_1V_2O_6$, X = 2 for $Cu_2V_2O_7$, X = 3 for $Cu_3V_2O_8$, and X = 5 for $Cu_5V_2O_{10}$. Typically, 1.5 mmol of Cu (Cu $(NO_3)_2{\cdot}3H_2O$) and the V precursors (NH_4VO_3 of 3 mmol for Cu_1, 1.5 mmol for Cu_2, 1 mmol for Cu_3, and 0.6 mmol for Cu_5) were dissolved in 70 and 170 mL deionized water, respectively. The Cu solution was then added dropwise to the V solution and stirred for an hour prior to the addition of 6 g of DT51. The resulting mixture was further stirred for 4 h, subjected to rotary evaporation to eliminate deionized water, and dried at 110 °C overnight. The resulting synthetic mixture was then calcined at 500 °C for 5 h at a ramp rate of 5 °C min^{-1} and cooled to room temperature. A series of Sb-promoted Cu_3/DT51 catalysts were synthesized following an identical protocol except that Sb dispersed on DT51 was used as the support during catalyst syntheses. For the syntheses of Sb-containing DT51, denoted as Sb_Y/DT51 [39,41,43], a pre-determined amount of the Sb precursor was typically dissolved in 500 g of acetic acid to form an Sb solution of $Sb(CH_3COO)_3$: 1.23 g for $Sb_{0.4}$/DT51, 2.45 g for $Sb_{0.9}$/DT51, 3.68 g for $Sb_{1.4}$/DT51, and 6.14 g for $Sb_{2.9}$/DT51. A pre-determined amount of DT51 was then added to the Sb solution and stirred overnight (DT51 of 49.5 g for $Sb_{0.4}$/DT51, 49 g for $Sb_{0.9}$/DT51, 48.5 g for $Sb_{1.4}$/DT51, and 47.5 g for $Sb_{2.9}$/DT51). Acetic acid was eliminated from the synthetic mixture by rotary evaporation. Subsequently, the synthetic mixture was dried at 110 °C overnight and calcined under identical conditions to those used to form Cu_3/DT51. The resulting Sb-promoted catalysts are denoted as Cu_3-Sb_Y/DT51, where Y indicates the observed Sb content (wt. %) in the catalysts such as 0.4, 0.9, 1.4, and 2.9. The catalysts were sulfated at 500 °C for 45 min in 500 ppm SO_2/3 vol. % O_2 balanced by N_2 at a total flow rate of 500 mL min^{-1} and a ramp rate of 10 °C min^{-1}. This led to the formation of Cu_X/DT51 (S) and Cu_X-Sb_Y/DT51 (S).

2.3. Synthesis of a simulated commercial catalyst

The control sample simulating a commercial catalyst was synthesized and targeted to include an almost identical V content to those for Cu_3-Sb_Y/DT51 (*i.e.*, 2.1 (± 0.1) wt. % V) [39,41,43]. Typically, 0.46 g of NH_4VO_3, 0.67 g of $(NH_4)_6H_2W_{12}O_{40}{\cdot}_XH_2O$, and 0.84 g of $C_2H_2O_4{\cdot}2H_2O$ were dissolved in 100 g of deionized water. Then, 9.3 g of DT51 was added to the precursor solution, stirred overnight, rotary evaporated, and calcined under identical conditions to those used to synthesize Cu_X/DT51.

2.4. Characterizations

N_2 physisorption experiments were performed using ASAP 2010 (Micromeritics) at 77 K to assess the textural properties of the catalysts after their degassing at 150 °C for 2 h under vacuum (*c.a.*, 4×10^{-9} mmHg). Brunauer-Emmett-Teller (BET) surfaces (S_{BET}) of the catalysts were determined using the amount of N_2 physisorbed on the catalyst surface at partial N_2 pressures of 0.05-0.3. Barrett-Joyner-Halenda (BJH) method served to evaluate the pore volumes of the catalysts, assuming that all pores were cylindrical. X-ray diffraction (XRD) patterns of the catalysts were acquired using D8 Advance (Bruker) with monochromatic CuKα radiation (λ = 0.154 nm) under the following condition: 2θ range of 20-80°; a scan speed of 2 s per step or 4 s per step; a step size of 0.02° per step. X-ray fluorescence (XRF) analyses of the catalysts were performed using ZSX Primus II (Rigaku) to quantify their bulk compositions. Titan 80-300™ (FEI) operated at 300 keV was used to obtain morphological/structural information of the catalyst surfaces using high resolution transmission electron microscopy (HRTEM) images, high angle annular dark field-scanning transmission electron microscopy (HAADF-STEM) images, and selected area electron diffraction (SAED) patterns. Prior to analyses, the catalyst was mixed with acetone, sonicated, dropped onto a holey carbon film grid, and dried at 40 °C under vacuum (*c.a.*, 2×10^{-7} torr). Following a similar procedure to that detailed in our previous works [45–49], we used Autochem II (Micromeritics) to perform CO-pulsed chemisorption experiments at 50 °C, before which the catalyst surface was purged with 5 vol. % O_2/He at 400 °C for an hour. X-ray photoelectron (XP) spectroscopy analyses of the catalysts were conducted using PHI 5000 VersaProbe after the catalyst surface had been cleaned under ultra-high vacuum (*c.a.*, 2×10^{-7} Pa). Adventituous carbon whose binding energy was centered at 284.6 eV served as a reference to characterize the catalyst surfaces. NH_3-temperaure programmed desorption (NH_3-TPD) and SO_2-temperaure programmed desorption (SO_2-TPD) experiments of the catalysts were performed using AutoChem II equipped with on-line mass spectrometer (HPR20, Hiden Analytical). Prior to the NH_3-TPD experiments, the catalysts were pre-treated with 10 vol. % O_2/He at 300 °C for an hour, cooled to 50 °C under a He atmosphere, exposed to 5 vol. % NH_3/He atmosphere at 50 °C for an hour to saturate the surface with NH_3, and heated to 600 °C at a ramp rate of 10 °C min^{-1}. The amount of NH_3-accessible sites present in the catalyst was evaluated using the NH_3 concentration (m/z = 17) *versus* temperature profile. Prior to SO_2-TPD analyses, the catalyst were pre-treated with 10 vol. % O_2/He at 300 °C for an hour, cooled to 250 °C under a He atmosphere, exposed to 5 vol. % SO_2/He atmosphere at 250 °C for an hour to populate the surface with SO_2, and heated to 900 °C at a ramp rate of 10 °C min^{-1}. The amount of SO_2 released from the catalyst surface was evaluated using the SO_2 concentration (m/z = 64) *versus* temperature profile. H_2-temperaure programmed reduction (H_2-TPR) experiments of the catalysts were also performed using AutoChem II, where the catalyst surface was purged with an Ar at 300 °C for an hour, cooled to 50 °C under an Ar atmosphere, and then heated to 900 °C under 10 vol. % H_2/He atmosphere at a ramp rate of 10 °C min^{-1}. The amount of H_2-accessible sites present in the catalyst was assessed from the thermal conductivitiy detector signal *versus* temperature profile. *In situ* diffuse reflectance infrared Fourier transform spectroscopy (DRIFT) experiments on the catalysts were performed using FT/IR/4200 (Jasco) with KBr optics and a mercury-cadmium-telluride (MCT) detector cooled by liquid N_2. The reaction cell (Harrick Scientific) loaded with the catalyst was connected to O_2, N_2, NO, and NH_3 gas flows with mass flow regulators. The catalyst in the cell was exposed to O_2/N_2 mixture at 400 °C for an hour, and then cooled to 250 °C. The background spectra of the catalysts at 250 °C were then collected under a N_2 atmosphere before recording a series of spectra with a resolution of 4 cm^{-1} under dynamic atmospheres of NO/O_2 or NH_3 at pre-determined time intervals. The details of the DRIFT experiments were given in Section 3.4 and Fig. 13 caption.

2.5. NH_3-SCR experiments

A fixed bed quartz reactor with an inner diameter of 0.8 cm was vertically positioned inside the furnace, and NH_3-SCR runs were performed at controlled reaction temperatures. All feed gas streams were regulated by a series of mass flow controllers to satisfy the following gas composition: 800 ppm NO, 800 ppm NH_3, 3 vol. % O_2, 6 vol. % H_2O (when necessary), and 500 ppm SO_2 (when necessary) balanced by N_2 with a total flow rate of 500 mL min^{-1}. Prior to conducting NH_3-SCR, ~0.31 g of the catalyst sieved to 300–425 μm (0.5 mL) was loaded into the quartz reactor to obtain a gas hourly space velocity as 60,000 h^{-1}. The catalyst was purged with 3 vol. % O_2/N_2 at 500 °C for an hour at a total flow rate of 500 mL min^{-1}. All gases during NH_3-SCR were monitored using on-line gas analyzers such as ZKJ-2 (Fuji Electric Co.) for NO and SO_2, and Ultramat 6 (Siemens Co.) for N_2O. Detector tubes (GASTEC Co.) were also used to measure the concentrations of NH_3 and NO_2 effluents. NO_X conversions (X_{NOX}) and N_2 selectivities (S_{N2})

obtained during NH_3-SCR were calculated according to Eqs. (1) and (2), where $C_{i,\ IN}$ and $C_{i,\ OUT}$ indicate the concentrations of species i at the inlet and outlet, respectively.

$$X_{NOX}\ (\%) = \frac{C_{NO,IN} - C_{NO,OUT} - C_{NO2,OUT} - 2 \times C_{N2O,OUT}}{C_{NO,IN}} \times 100 \quad (1)$$

$$S_{N2}\ (\%) = \frac{C_{NO,IN} + C_{NH3,IN} - C_{NO,OUT} - C_{NH3,OUT} - C_{NO2,OUT} - 2 \times C_{N2O,OUT}}{C_{NO,IN} + C_{NH3,IN} - C_{NO,OUT} - C_{NH3,OUT}} \times 100 \quad (2)$$

3. Results and discussion

3.1. Copper vanadates on DT51

Anatase (DT51)-supported copper vanadate catalysts with four different phases were synthesized *via* a wet-impregnation protocol, after which they were subjected to calcination at 500 °C for the generation of the target phases (*i.e.*, Cu_1, Cu_2, Cu_3, and Cu_5) [32–34]. The selection of DT51 (anatase) as a support was based on 1) its meso-porosity, which was beneficial for NO_X/NH_3 diffusion, 2) the high dispersion of copper vanadates, and 3) the inclusion of abundant labile oxygen species, which promoted redox cycles during NH_3-SCR [26,50,51]. The resulting catalysts are denoted as Cu_X/DT51, where X can be 1, 2, 3, or 5. X-ray diffraction (XRD) served to identify the bulk phases of the catalysts, all of which had typical bulk crystal planes assigned to *tetragonal* anatase, originating from the DT51 support (JCPDF No. of 01-084-1285 in Fig. 2(a)). In addition, Cu_1/DT51, Cu_2/DT51, and Cu_3/DT51 contained reflections corresponding to *monoclinic* Cu_1 ($Cu_1V_2O_6$; JCPDF No. of 01-074-2117), Cu_2 ($Cu_2V_2O_7$; JCPDF No. of 01-073-1032), and Cu_3 ($Cu_3V_2O_8$; JCPDF No. of 00-026-0567). Cu_5/DT51, however, did not exhibit any reflections corresponding to *monoclinic* Cu_5 ($Cu_5V_2O_{710}$; JCPDF No. of 00-027-1135) in the XRD pattern. To verify the formation of Cu_5, Cu_5/DT51 was analysed using selected area electron diffraction (SAED), in which reflections indicating Cu_5 were present such as (−1 1 1) and (−2 1 2) with d spacings of ~4.9 Å and ~3.4 Å, respectively (Fig. 2(c)). Although the (−2 1 2) reflection of Cu_5 could also be assigned to the (1 0 1) reflection of anatase because of their similar d values (*i.e.*, ~3.5 Å), the (−1 1 1) reflection of Cu_5, however, was missing from the SAED pattern of DT51 (Fig. 2(b)). This results suggested Cu_5 particles were successfully deposited onto the surface of Cu_5/DT51.

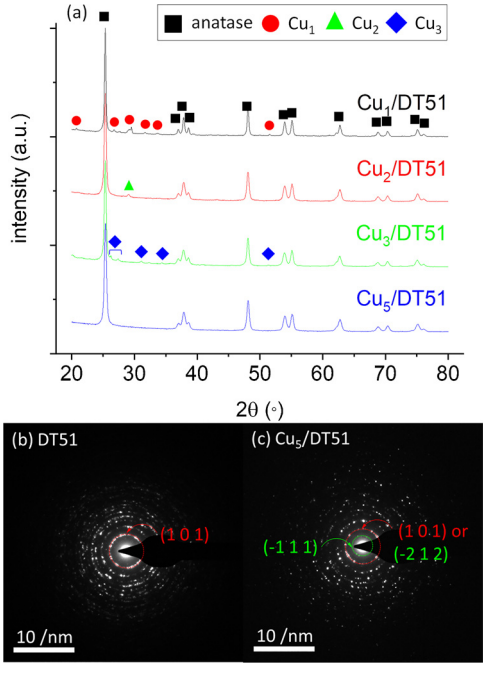

Fig. 2. (a) XRD patterns of Cu_X/DT51 catalysts. SAED patterns of (b) DT51 and (c) Cu_5/DT51. Parentheses in (b) and (c) indicate crystal facets for anatase (red-colored) or Cu_5 (green-colored). Other facets indicating Cu_5 or DT51 are omitted due to similar d spacings. (For interpretation of the references to colour in this figure legend, the reader is referred to the web version of this article).

Table 1
Properties of copper vanadates on DT51.

catalyst	contents				S_{BET} [d,e] ($m^2\ g^{-1}$)	V_{PORE} [d,f] ($cm^3\ g^{-1}$)
	Cu [a] (wt. %)	V/Cu [b]				
		theoretical	bulk [a]	surface [c]		
Cu_1/DT51	4.1	2.0	1.9	3.0	15	0.1
Cu_2/DT51	4.3	1.0	1.0	1.5	38	0.2
Cu_3/DT51	4.4	0.7	0.7	1.1	44	0.2
Cu_5/DT51	4.4	0.4	0.4	0.6	49	0.3

[a] *via* XRF.
[b] molar ratio.
[c] *via* XPS.
[d] *via* N_2 physisorption.
[e] *via* BET.
[f] *via* BJH.

Of note, the catalysts were synthesized using an identical amount of Cu, but utilizing different amounts of V, which was determined based on the stoichiometry of copper vanadates (*e.g.*, V:Cu molar ratio of 2:3 for $Cu_3V_2O_8$). The bulk V and Cu compositions of the catalysts were evaluated *via* X-ray fluorescence (XRF). The results showed that the catalysts had a consistent Cu content (4.3 (± 0.1) wt. %) with V contents consistent with the theoretical molar ratios of V to Cu (V/Cu in Table 1). Therefore, we expected that the catalysts with greater V/Cu would have lower porosities because of higher V contents inside the pores of DT51. This was evidenced by N_2 physisorption experiments for the catalysts, which revealed Cu_1/DT51 with the greatest V/Cu ratio had the smallest Brunauer-Emmett-Teller (BET) surface area as well as pore volume among the catalysts (Table 1). To perform morphological observations of the catalysts, we used high-resolution transmission electron microscopy (HRTEM). As shown in the HRTEM images, the catalysts comprised metal oxide aggregates with sizes of 0.5–1 μm and exhibited lattice fringes indicating either copper vanadates or anatase (Fig. 3(a)–(h) and Fig. S2(a)–(b)). The particle sizes of copper vanadates were then evaluated using high angle annular dark field-scanning transmission electron microscopy (HAADF-STEM). HAADF-STEM images of the catalysts showed copper vanadate particles that were discernible as white spots with sizes of ≤ ~2 nm and were dispersed throughout the DT51 (Fig. 3(i)–(l)). This dispersion was evident because the HAADF-STEM image of DT51 did not contain such ~2 nm-sized particles on its surface (Fig. S2 (c)). All of these experiments provided evidence that small copper vanadate particles with the desired crystal phases had been deposited on DT51.

X-ray photoelectron (XP) spectroscopy was employed to explore surface properties of the catalysts. The surfaces had greater surface molar ratios of V to Cu than the bulk molar ratio counterparts (Table 1), which suggested vanadium oxide species (VO_X) were enriched on the surfaces. Previous studies on $FeVO_4$ have also validated that the surface-rich VO_X species acted as major active sites for NH_3-SCR [30], as might be the case with the Cu_X/DT51 catalysts synthesized in this work. All the catalysts primarily incorporated the surface Ti^{4+} and V^{5+} species. This was evidenced by XP spectra of the catalysts, all of which contained peaks with binding energies centered at ~458.7 eV and ~517 eV in Ti 2p $_{3/2}$ and V 2p $_{3/2}$ regimes, respectively (Fig. S1). The catalysts had surface Cu^{2+} and Cu^{+} species, as corroborated by two sub-bands with binding energies centered at ~934.2 eV and ~932.1 eV, respectively (Fig. 4(a)) [30,34,52,53]. The abundance of surface Cu^{+}/Cu^{2+} species in the catalysts varied according to the

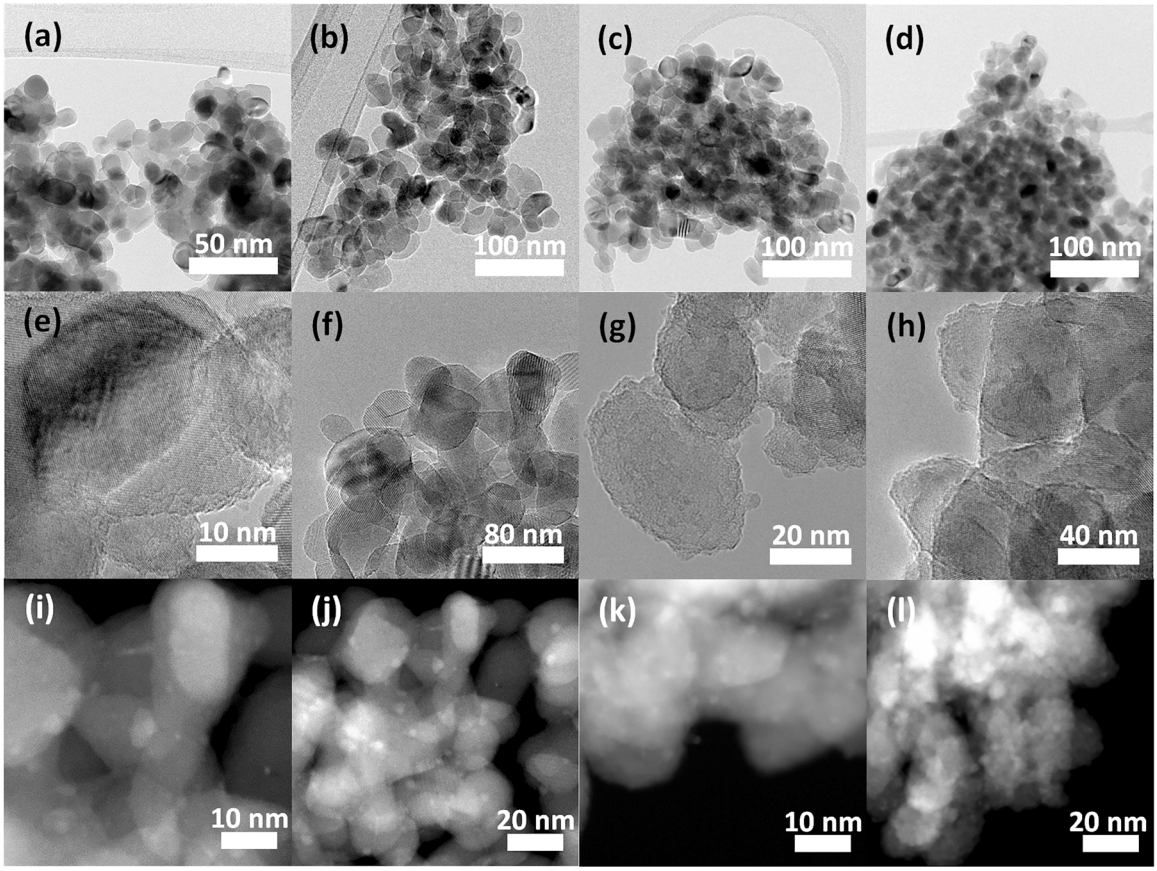

Fig. 3. HRTEM images of Cu_X/DT51 catalysts with low (a–d) and high magnifications (e-h) and HAADF-STEM images of Cu_X/DT51 catalysts (i–l): a, e, and i for Cu_1/DT51; b, f, and j for Cu_2/DT51; c, g, and k for Cu_3/DT51; d, h, and l for Cu_5/DT51.

change in the type of Cu_X deposited on the surface of DT51. Noteworthy, the highest abundance of Cu^+ species was observed in Cu_1/DT51, which was interesting concerning the analysis of the NH_3-SCR performance of the catalysts. The O 1 s regimes in XP spectra of the catalysts showed three major sub-bands post fitting (Fig. 4(b)). These peaks were located at ~530 eV, ~531 eV, and ~525.5 eV and were assigned to lattice oxygen (O_β), surface labile, mobile oxygen (O_α; *e.g.*, O_2^{2-} or −OH), and chemisorbed H_2O (O_α'), respectively [44,52]. The abundance of O_α increased in the following order of $Cu_1 \rightarrow Cu_2 \rightarrow Cu_3 \rightarrow Cu_5$. This suggested Cu_5 could exhibit the greatest redox character while accelerating NO oxidation to form NO_2, which is favorable for the 'fast SCR' during NH_3-SCR [30,42,44,54,55]. This result, hence, substantiated our hypothesis that different atom connectivities of the copper vanadates can vary the redox characters of the resulting catalysts, which were distinct from one another.

The redox feature of the catalysts were further analyzed *via* H_2-temperature programmed reduction (H_2-TPR), where Cu_1/DT51 showed greater H_2 consumption than the others, as evidenced by the H_2-TPR profiles of the catalysts (Fig. 5(a)). Cu_1/DT51, however, consumed H_2 primarily above 300 °C (~3.2 $mmol_{H2}$ g^{-1}), which suggested that Cu_1/DT51 might not significantly promote NH_3-SCR performance at low temperatures (*i.e.*, ≤ 300 °C). Most of the H_2 consumptions

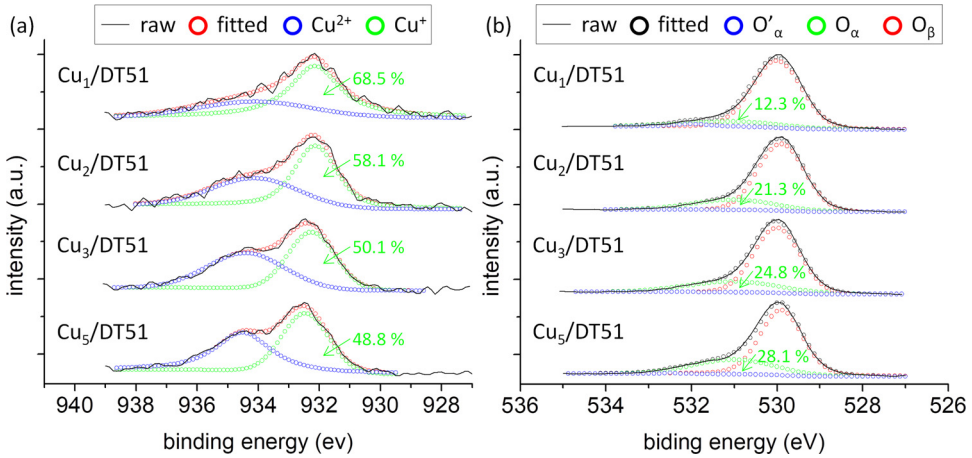

Fig. 4. XP spectra of Cu_X/DT51 catalysts: (a) Cu 2p $_{3/2}$ and (b) O 1 s regimes. Green numbers with arrows in (a) and (b) indicate abundance of surface Cu^+ and labile oxygen (O_α) species, respectively (For interpretation of the references to colour in this figure legend, the reader is referred to the web version of this article).

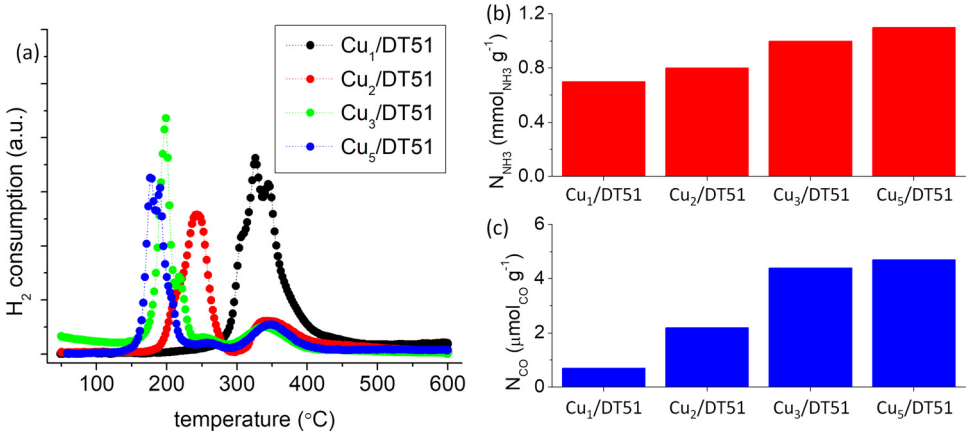

Fig. 5. (a) H_2-TPR profiles, (b) the amount of total acid sites (N_{NH3}), and (c) the amount of Lewis acid sites (N_{CO}) of Cu_X/DT51 catalysts.

occurred at ≤ 300 °C for the other catalysts, among which Cu_2/DT51 showed enhanced H_2 consumption compared to Cu_3/DT51 and Cu_5/DT51 (~1.8 $mmol_{H2}$ g^{-1} for Cu_2/DT51, ~1.3 $mmol_{H2}$ g^{-1} for Cu_3/DT51, and ~1.7 $mmol_{H2}$ g^{-1} for Cu_5/DT51). Cu_2/DT51, yet, showed the highest H_2 consumption at ~250 °C and thus might not be as effective as Cu_3/DT51 and Cu_5/DT51 for facilitating redox cycle during NH_3-SCR at 150–250 °C.

The acid character of the catalysts was also evaluated *via* NH_3-temperature programmed desorption (NH_3-TPD) experiments. The catalysts showed wide temperature ranges to desorb NH_3 (100–600 °C) with no distinct peaks that could be assigned to Brönsted or Lewis acid sites (Fig. S3 (a)). Despite literature reports assigning or quantifying Brönsted or Lewis acid sites based on their NH_3 desorption temperatures, the deconvolution of these sites in a rigorous manner is challenging due to presence of the strong Brönsted acid or weak Lewis acid sites present in the catalysts [56,57]. We therefore could only quantify the total amount of acid sites present in the catalysts. As shown in Fig. 5(b), Cu_X/DT51 with a large value of X had increased number of total acid sites (N_{NH3}), which validated the different atom connectivites of copper vanadates affected the total amount of acid sites. Obviously, Cu_1/DT51 had the lowest N_{NH3} among the tested catalysts, partially resulting from the absence of Lewis acid sites available to bind with NH_3 species, as discussed above [33,34]. To further demonstrate this, we also utilized CO as a probe molecule because of its property to bind only with the coordinatively unsaturated Lewis acid sites present in the catalyst surface [45–49]. We thus performed CO-pulsed chemisorption experiments to assess the amount of CO-accessible sites (N_{CO}) present in the catalysts. Interestingly, the N_{CO} values of the catalysts were detected about 10^{-3} times lower than their corresponding N_{NH3} values. This was probably because the accessibility of catalytic sites was dependent on the type of a probe molecule. However, as anticipated, Cu_1/DT51 had the smallest N_{CO} value among all the catalysts (Fig. 5(c)).

The surface characterization results suggested Cu_X/DT51 with a large X value should perform NH_3-SCR well. This was validated by a series of experiments to measure NH_3-SCR performance of the catalysts such as NO_X conversion (X_{NOX}) and N_2 selectivity (S_{N2}) in the absence of H_2O and SO_2. While including 5 wt. % W, a control simulating a commercial VO_X-based catalyst was prepared for comparison with Cu_X/DT51: This control is denoted as V_2O_5-WO_3/TiO_2. V content in V_2O_5-WO_3/TiO_2 was set to 2 wt. % because Cu_3/DT51 with ~2 wt. % V outperformed the other CU_X/DT51 catalysts during NH_3-SCR in the presence of H_2O and SO_2, which was discussed in a later section. As shown in Fig. 6, Cu_5/DT51 showed the highest X_{NOX} and S_{N2} (≥ ~90%) among the Cu_X/DT51 catalysts at ≤ 250 °C, which, again, could be caused by the largest quantities of total acid sites and labile oxygen species with good redox feature at ≤ 250 °C. Notably, the Cu_5/DT51 had the greatest abundance of surface Cu^{2+} species among the

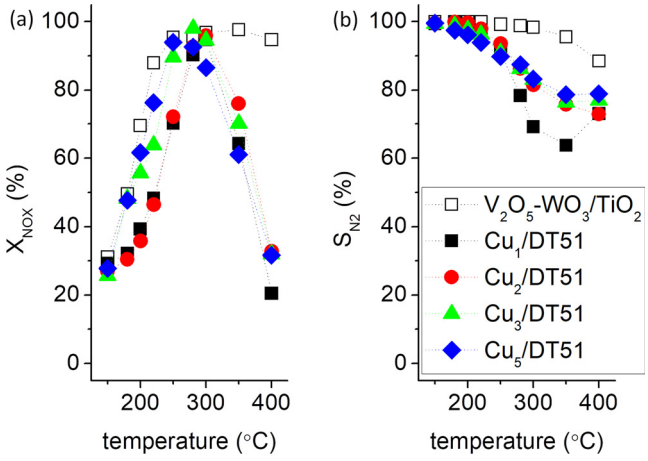

Fig. 6. NH_3-SCR performance of V_2O_5-WO_3/TiO_2 and Cu_X/DT51 catalysts: (a) NO_X conversion (X_{NOX}) *versus* reaction temperature and (b) N_2 selectivity (S_{N2}) *versus* reaction temperature. Reaction condition: 800 ppm NO_X; 800 ppm NH_3; 3 vol. % O_2; total flow rate of 500 mL min^{-1}; space velocity of 60,000 h^{-1}; balanced by N_2.

catalysts (Fig. 4(a)) and this might partially contribute to the promotion of the NH_3-SCR performance of Cu_5/DT51. Even with its good NH_3-SCR performance at low temperatures, Cu_5/DT51 showed NH_3-SCR performance inferior to V_2O_5-WO_3/TiO_2 at ≥ 200 °C and exhibited an abrupt decrease in both X_{NOX} and S_{N2} at ≥ 280 °C. This behavior was partly a result of the presence of acid sites that could interact with and oxidize NH_3 species to generate NO_X and N_2O species [58,59].

3.2. Copper vanadates on DT51 with sulfation

Note that the NH_3-SCR reaction runs in Fig. 6 were conducted in the absence of H_2O and SO_2, both of which are the major components in the flue gas emitted from diesel fuel combustion such as coal-fired plants and diesel engines [14–17]. As discussed in the introduction, the catalyst should be tolerant to ammonium (bi) sulfate (ABS) species during the NH_3-SCR for long-term stability [37–41]. To test the ABS resistance of the catalysts, we exposed the catalyst surfaces to SO_2 and O_2 under a controlled environment (denoted as sulfation). The control condition was identical to that used during the initial NH_3-SCR run in the presence of SO_2 and O_2 at 500 °C except that NO_X, NH_3, and H_2O were not added to the feed stream. This led to the formation of a series of catalysts denoted as Cu_X/DT51 (S), where X values were 1, 2, 3, and 5.

XRD analysis of the sulfated catalysts showed almost identical patterns compared to those of the catalysts prior to sulfation (not shown). This suggested that 1) a high dispersion of copper vanadate particles on

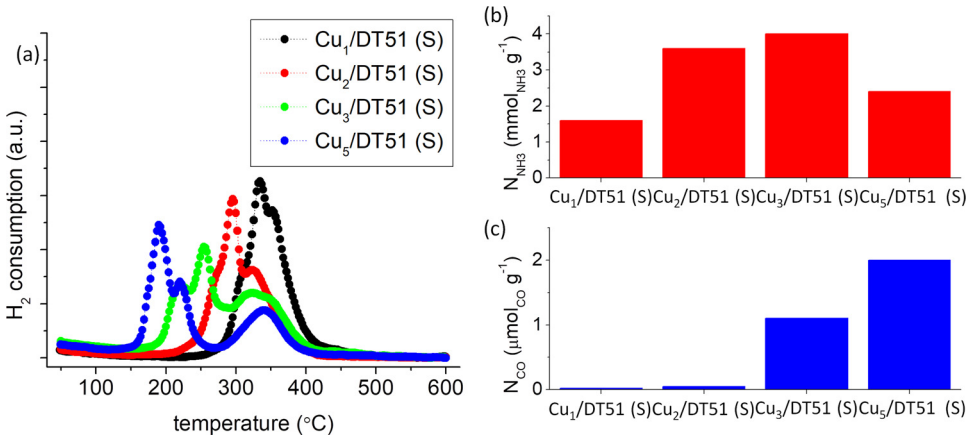

Fig. 7. (a) H_2-TPR profiles, (b) the amount of total acid sites (N_{NH3}), and (c) the amount of Lewis acid sites (N_{CO}) of Cu_X/DT51 (S) catalysts.

the DT51 surface was highly likely and 2) there was no noticeable change in the copper vanadate bulk crystal structures post sulfation. Redox feature of the catalysts post sulfation was evaluated *via* H_2-TPR experiments (Fig. 7(a)). After sulfation, Cu_1/DT51 (S) still consumed the largest quantity of H_2 among the catalysts although Cu_1/DT51 (S) was significantly reduced at elevated temperatures (*i.e.*, > 300 °C). While retaining the reduction temperatures below 300 °C, the other sulfated catalysts showed promoted redox feature compared to their unsulfated analogues. The increased H_2 consumption in the sulfated catalysts was quantified as 0.7 $mmol_{H2}$ g^{-1} for Cu_2/DT51 (S), 1.3 $mmol_{H2}$ g^{-1} for Cu_3/DT51 (S), and 0.3 $mmol_{H2}$ g^{-1} for Cu_5/DT51 (S), indicating that Cu_3/DT51 (S) possessed the greatest redox ability.

Sulfation has been reported to be a feasible way to generate additional Brönsted acid site on catalyst surfaces [41–44]. Therefore, compared to the fresh catalysts, their sulfated counterparts required larger H_2 quantities to fully reduce the surfaces, including sulfation-driven Brönsted acid sites (*i.e.*, S−OH) [41–44]. This was evidenced by NH_3-TPD profiles of the sulfated catalysts, which showed a substantial increase in the quantities of NH_3-accessible sites (*i.e.*, N_{NH3}) over the unsulfated analogues (Fig. 7(b) and S3 (b)). Notably, Cu_3/DT51 (S) was found to have the largest N_{NH3} among the sulfated catalysts. The increase in the amount of Brönsted acid sites in the sulfated catalysts was further confirmed by CO-pulsed chemisorption results (Fig. 7(c)). This showed all sulfated catalysts contained far fewer CO-accessible Lewis acid sites in comparison with those of the unsulfated counterparts. In contrast, Cu_3/DT51 (S) and Cu_5/DT51 (S) contained Lewis acid sites that were still accessible to CO. These experiments highly suggested Cu_3/DT51 (S) had the greatest NH_3-SCR performance among the sulfated catalysts.

These catalysts were tested for NH_3-SCR with the addition of H_2O and SO_2 to the feed stream to simulate industrial flue gas (Fig. 8). Noteworthy, the catalysts were indispensably sulfated at 500 °C to obtain a consistent NH_3-SCR performance at 500 °C. This took 45 min, the same time for producing Cu_X/DT51 (S). The choice of 500 °C as the sulfation temperature was based on our previous studies, which had shown that catalyst sulfated at 500 °C could achieve better SCR performance than those sulfated at < 500 °C [43,44]. Even though the sulfated catalysts contained larger amounts of acid sites than their unsulfated analogues, the sulfated catalysts showed lower NO_X conversion at ≤ 300 °C in comparison with their unsulfated counterparts. This was indicative of the tolerance of the catalysts to SO_2 and ammonium (bi) sulfates, which was paramount for the retention or the improvement in their SCR performance in the presence of H_2O and SO_2 during NH_3-SCR. Nevertheless, the N_2 selectivities (S_{N2}) of the sulfated catalysts were improved compared to their unsulfated analogues, particularly, at elevated temperatures (*i.e.*, ≥ 280 °C). This was attributed to the H_2O in the stream fed during NH_3-SCR, which could coordinate

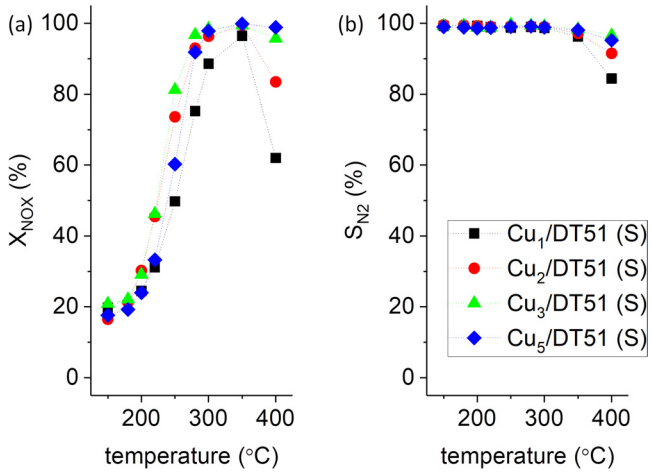

Fig. 8. NH_3-SCR performance of Cu_X/DT51 (S) catalysts: (a) NO_X conversion (X_{NOX}) *versus* reaction temperature and (b) N_2 selectivity (S_{N2}) *versus* reaction temperature. Reaction condition: 800 ppm NO_X; 800 ppm NH_3; 3 vol. % O_2; 6 vol. % H_2O; 500 ppm SO_2; total flow rate of 500 mL min^{-1}; space velocity of 60,000 h^{-1}; balanced by N_2.

to the strong Brönsted acid sites present in the sulfated catalyst, thereby suppressing NH_3 oxidation [60–62]. As expected based on characterization experiments of all catalysts post sulfation, the best NH_3-SCR performance was achieved on the sulfated Cu_3/DT51. This again corroborated our hypothesis concerning the optimum copper vanadate structure for obtaining great NO_X conversion, N_2 selectivity, and ABS tolerance during NH_3-SCR at ≤ 400 °C.

3.3. Sb-promoted copper vanadates on DT51 with sulfation

Utilizing the optimized active sites (*i.e.*, Cu_3), we then synthesized another series of catalysts using DT51 with various Sb quantities as supports. (See the Experimental section for details.) These are denoted as Cu_3-Sb_Y/DT51, where Y indicates Sb content (wt. %) obtained *via* XRF (*i.e.*, Y = 0.4, 0.9, 1.4. or 2.9). The morphology of the Cu_3-$Sb_{1.4}$/DT51 was analyzed using HRTEM and HAADF-STEM images, wherein copper vanadate and Sb oxide with diameters of ≤ ~2 nm were found and dispersed on 0.5–1 μm-sized anatase aggregates (Fig. S4(a)–(c)). The SAED pattern of Cu_3-$Sb_{1.4}$/DT51 also showed facets corresponding to Cu_3 ((1 0 0) with a *d* value of ~5.8 Å) or Sb_2O_5 ((1 1 1) with a *d* value of ~6.0 Å). These facets did not overlap with those of DT51 (*i.e.*, (1 0 1) with a *d* value of ~3.5 Å)), thereby suggesting the successful synthesis of Cu_3-$Sb_{1.4}$/DT51 (Fig. S4 (d)).

Cu_3-Sb_Y/DT51 catalysts were also sulfated under identical

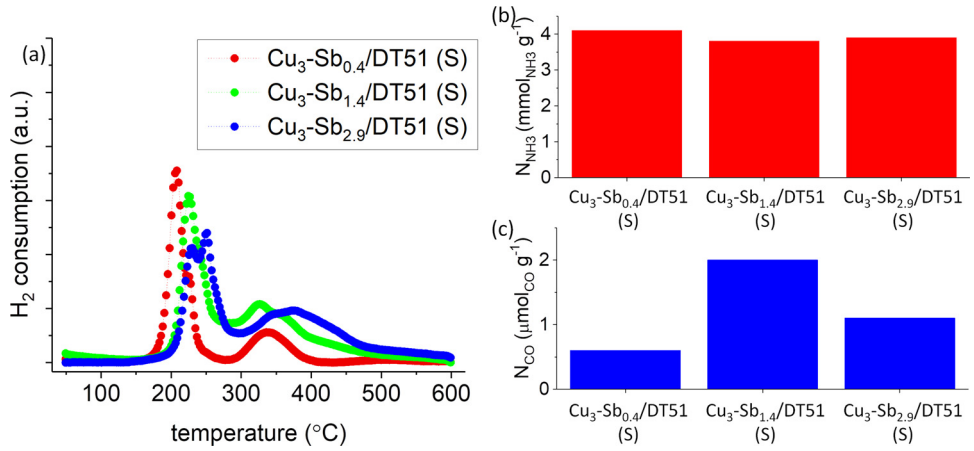

Fig. 9. (a) H_2-TPR profiles, (b) the amount of total acid sites (N_{NH3}), and (c) the amount of Lewis acid sites (N_{CO}) of Cu_3-Sb_Y/DT51 (S) catalysts.

conditions to that used to produce CU_3/DT51 (S), leading to the generation of Cu_3-Sb_Y/DT51 (S). Of note, Cu_3-$Sb_{0.9}$/DT51 (S) had similar properties to those of Cu_3-$Sb_{1.4}$/DT51 (S) and thus was omitted from the following discussion for simplicity. As shown in Fig. 9(a), all Cu_3-Sb_Y/DT51 (S) catalysts primarily consumed H_2 at low temperatures (*i.e.*, 200–300 °C), which was similar behavior to that observed for Cu_3/DT51 (S). Significant differences were found in the amount of H_2 needed to reduce the surfaces during the H_2-TPR experiments, where Cu_3-$Sb_{1.4}$/DT51 (S) (3.4 $mmol_{H2}$ g^{-1}) and Cu_3-$Sb_{2.9}$/DT51 (S) (3.1 $mmol_{H2}$ g^{-1}) consumed greater H_2 quantities than Cu_3/DT51 (S) (2.6 $mmol_{H2}$ g^{-1}). This suggested that the inclusion of the optimum amount of Sb into the copper vanadate catalyst (Cu_3-$Sb_{1.4}$/DT51 (S)) could enhance the redox character compared to that of the bare catalyst (Cu_3/DT51 (S)). Furthermore, the addition of Sb increased the quantity of Lewis acid sites in Cu_3-Sb_Y/DT51 (S) compared to Cu_3/DT51 (S) particularly when the optimum amount of Sb was added (*i.e.*, Cu_3-$Sb_{1.4}$/DT51 (S) in Fig. 9(c)). However, even after the inclusion of Sb, the Cu_3-Sb_Y/DT51 (S) catalysts had similar amounts of total acid sites to that of Cu_3/DT51 (S) (Fig. 9(b)), which indicated that Sb promoter might not substantially aid in improving the acid character of the catalysts. The SO_2-temperature programmed desorption (SO_2-TPD) experiments, however, corroborated that the inclusion of Sb into the catalysts could help suppress the interactions among SO_2 species and the catalyst surface. Cu_3/DT51 and Cu_3-$Sb_{1.4}$/DT51 served as model catalysts and their surfaces were saturated with SO_2 species at 250 °C post purging the surfaces. The amount of SO_2 escaped from the surfaces with temperature change was recorded, as shown in Fig. 10. Both catalysts showed similar trends concerning the release of SO_2 species with increasing temperature. These catalysts showed three peaks at temperatures centered at ~350 °C, ~620 °C, and ~660 °C, among which a temperature of > 600 °C was required to liberate the SO_2 species chemisorbed on the surfaces, as conjectured based on previous studies [63–66]. Of significant importance was the amount of SO_2 released from the surfaces, where Cu_3-$Sb_{1.4}$/DT51 liberated less SO_2 than Cu_3/DT51. This provided evidence associated with the role of Sb in reducing the formation of SO_3 and ABS species by diminishing the interactions of SO_2 species with the catalyst surface during NH_3-SCR.

All of the Cu_3-Sb_Y/DT51 catalysts were tested for NH_3-SCR with a reactant gas composition simulating flue gas and compared with Cu_3/DT51 (Figs. 8 and 11). Similar to the NH_3-SCR reaction runs of the Cu_X/DT51 catalysts in the presence of H_2O and SO_2, all Sb-promoted catalysts were 'sulfated' at 500 °C for 45 min prior to measuring the NH_3-SCR performance. Despite having a S_{N2} of ≥ 95% over a wide temperature regime, the X_{NOX} values were significantly enhanced in 'sulfated' Cu_3/DT51 with the inclusion of the Sb promoter. Of note, the increase in X_{NOX} values depended on the amount of Sb included in the Cu_3-Sb_Y/DT51 (S) catalysts. This was apparent in the NH_3-SCR performance of the catalysts at 250 °C, where the 'sulfated' Cu_3-Sb_Y/DT51 catalysts showed a 25–40 % increase in X_{NOX} values in comparison with

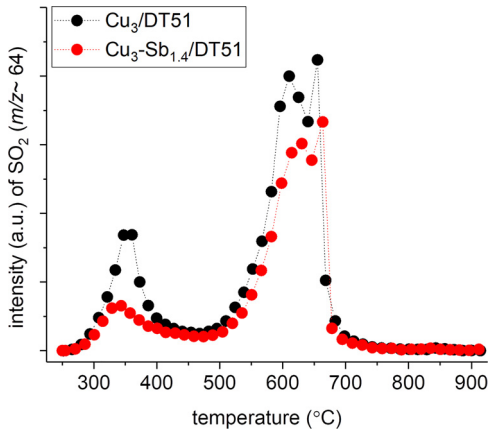

Fig. 10. SO_2-TPD profiles of Cu_3/DT51 and Cu_3-$Sb_{1.4}$/DT51 catalysts.

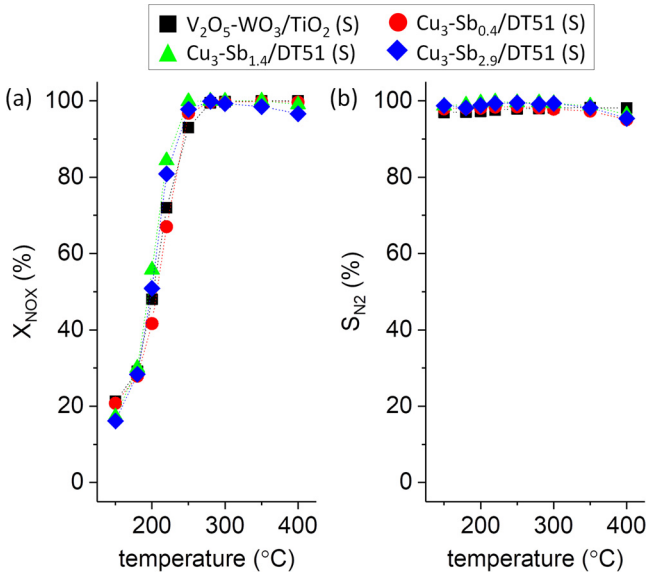

Fig. 11. NH_3-SCR performance of V_2O_5-WO_3/TiO_2 (S) and Cu_3-Sb_Y/DT51 (S) catalysts: (a) NO_X conversion (X_{NOX}) *versus* reaction temperature and (b) N_2 selectivity (S_{N2}) *versus* reaction temperature. Reaction condition: 800 ppm NO_X; 800 ppm NH_3; 3 vol. % O_2; 6 vol. % H_2O; 500 ppm SO_2; total flow rate of 500 mL min^{-1}; space velocity of 60,000 h^{-1}; balanced by N_2.

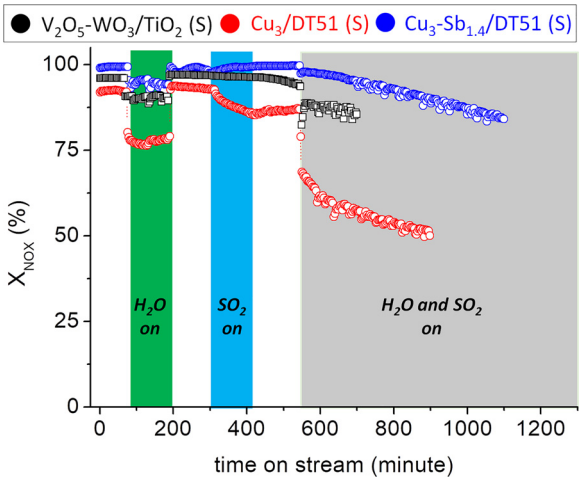

Fig. 12. NO_X conversion (X_{NOX}) *versus* time on stream of V_2O_5-WO_3/TiO_2 (S), Cu_3/DT51 (S), and Cu_3-$Sb_{1.4}$/DT51 (S) catalysts at 250 °C. Green- or light blue-shaded rectangles indicate the regimes where only H_2O or only SO_2 is fed to the reactor. Grey-shaded rectangle indicates the regime where both H_2O and SO_2 are supplied to the reactor. Reaction condition: 800 ppm NO_X; 800 ppm NH_3; 3 vol. % O_2; 6 vol. % H_2O; 500 ppm SO_2; total flow rate of 500 mL min^{-1}; space velocity of 60,000 h^{-1}; balanced by N_2. (For interpretation of the references to colour in this figure legend, the reader is referred to the web version of this article).

the X_{NOX} value of 'sulfated' Cu_3/DT51 (~45%). Of additional note, the properties of Cu_3-$Sb_{1.4}$/DT51 (S) were most favorable for NH_3-SCR among all catalysts synthesized herein and also led to the best NH_3-SCR performance. Importantly, 'sulfated' Cu_3-$Sb_{1.4}$/DT51 showed greater NH_3-SCR performance than 'sulfated' V_2O_5-WO_3/TiO_2. This again validated that optimizing the copper vanadate structure and Sb content would be an efficient way to create a high-performance catalyst for NH_3-SCR.

The long-term stability of Cu_3/DT51 and Cu_3-$Sb_{1.4}$/DT51 during NH_3-SCR was also tested and compared with the simulated commercial V_2O_5-WO_3/TiO_2 catalyst (Fig. 12). First, all catalysts were sulfated at 500 °C for 45 min, leading to the formation of Cu_3 /DT51 (S), Cu_3-$Sb_{1.4}$/DT51 (S), and V_2O_5-WO_3/TiO_2 (S) prior to the durability experiments. A reaction temperature of 250 °C was utilized for these experiments to evaluate their tolerance to either SO_2 or ABS species at low temperatures. The X_{NOX} values of all catalysts were initially stable but dropped by 10–15 % in the presence of H_2O, although they recovered to their original values when the flow of H_2O in the feed stream was halted. This behavior was expected because H_2O could compete with NH_3 for adsorption on the surface acid sites [67–69]. When SO_2 was fed to the reactor, the initial X_{NOX} values of both Cu_3-$Sb_{1.4}$/DT51 (S) and V_2O_5-WO_3/TiO_2 (S) levelled off. These X_{NOX} values were retained until just before H_2O and SO_2 were co-fed to the reactor, which suggested these two catalysts showed good resistance to SO_2. This performance contrasted with that of Cu_3 /DT51 (S), which exhibited a continuous reduction in X_{NOX} values of ~5% in the presence of SO_2 and did not recover the X_{NOX} values even in the absence of SO_2 and H_2O. In conjunction with the SO_2-TPD experiments discussed above, this demonstrated the benefit of Sb as a promoter to prevent the catalyst surface from interacting with SO_2, thereby minimizing surface poisoning by SO_2. The additional role of Sb as a promoter to avoid the surface interactions with ABS species was pronounced when SO_2 and H_2O were co-fed to the reactor. In the presence of SO_2 and H_2O, Cu_3/DT51 (S) showed a sudden decrease in the X_{NOX} value from ~85% to ~70% and the X_{NOX} value continuously reduced to ~50% over 6 h. In contrast to Cu_3/DT51 (S), Cu_3-$Sb_{1.4}$/DT51 (S) showed X_{NOX} values of ≥ ~85% up to ~9.5 h, which was far longer than the time required for V_2O_5-WO_3/TiO_2 (S) to reach X_{NOX} values of ~85% (*i.e.*, ~2.5 h). These experiments validated the roles of Sb in promoting tolerance to SO_2/ABS during NH_3-SCR and to improving redox character of the catalyst.

3.4. Surface reaction mechanism

The low-temperature surface NH_3-SCR mechanisms of Cu_3/DT51 (S), Cu_3-$Sb_{1.4}$/DT51 (S), and V_2O_5-WO_3/TiO_2 (S) were investigated *via* background-subtracted *in situ* diffuse reflectance infrared Fourier transform spectroscopy (DRIFT). A temperature of 250 °C was chosen for these experiments because of the substantial difference in the NH_3-SCR performance of these catalysts at 250 °C (Figs. 8 and 11). The catalyst surfaces were initially purged with O_2/N_2 at 400 °C and then cooled to 250 °C under a N_2 atmosphere prior to the collection of the background spectra of the surfaces. After subtracting the background signals, the surfaces were then exposed to 1000 ppm NO coupled with O_2/N_2 for 30 min. It was expected that NO and O_2 could co-adsorb onto the surfaces and form a variety of nitrate/nitrite species with *mono*-dentate, *bi*-dentate, or bridged binding configurations. However, the bands assigned as vibrations of surface-adsorbed nitrate/nitrite species were found to be minute for these catalysts (Fig. 13(a)–(c)). This provided evidence that the surfaces had little affinity for binding with NO and O_2.

Bands, however, were significantly developed and saturated within 30 min when the gaseous atmosphere on the surfaces was subsequently changed to 1000 ppm NH_3/N_2 (Fig. 13(d)–(f)). Importantly, these experiments demonstrated that the active sites on the surfaces were favorable for the coordination of NH_3 species rather than the interaction of NO or O_2. The bands located at ~1450 cm^{-1} and 1650–1800 cm^{-1} could be assigned to the symmetric and asymmetric N—H bending vibrations of NH^{4+} chemisorbed onto Brönsted acid sites (*i.e.*, metal—OH or S—OH, denoted as ***B***) [44,70–72]. In addition, the bands centered at

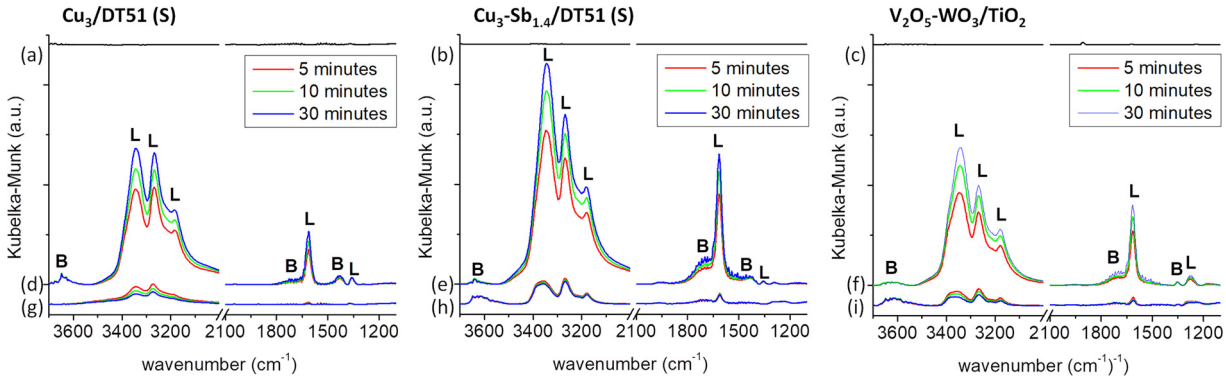

Fig. 13. Background-subtracted *in situ* DRIFT spectra of Cu_3/DT51 (S), Cu_3-$Sb_{1.4}$/DT51 (S), and V_2O_5-WO_3/TiO_2 (S) at 250 °C. Surfaces are purged under O_2/N_2 mixture at 400 °C for an hour. Surfaces are initially saturated with NO (1000 ppm) + O_2 (3 vol. %) for 30 min (a–c), sequentially saturated with NH_3 (1000 ppm) for 30 min (d–f), and then re-saturated with NO (1000 ppm) + O_2 (3 vol. %) for 30 min (g–i). Gases are balanced by N_2, while retaining a total flow rate of 200 mL min^{-1}.

~1360 cm^{-1} and ~1620 cm^{-1} could be assigned to the symmetric and asymmetric N—H bending vibrations of NH_3 chemisorbed onto Lewis acid sites (denoted as ***L***) [44,70,73]. Several bands were also found at > 3000 cm^{-1} in these spectra. A broad signal at 3600–3700 cm^{-1} could be attributed to the N—H stretching vibration of NH^{4+} on ***B*** sites, whereas three signals centered at 3100–3400 cm^{-1} could be ascribed to the N—H stretching vibrations of NH_3 on ***L*** sites [44,70].

An interesting feature was observed in these spectra, where the ***B*** bands exhibited far lower intensities than the ***L*** bands. The ***B*** sites present in CeO_2 on TiO_2 catalysts readily released NH_3 (or NH_4^+) species at ≥ 200 °C, as reported by M. Ge and co-workers [71]. This was in contrast to the ***L*** sites present in CeO_2 on TiO_2 showing NH_3 species were rigidly bound to the ***L*** sites even at 300 °C, as evidenced by the slight decrease in the intensities of the ***L*** bands at ≤ 300 °C [71]. The *in situ* DRIFT spectra of the catalysts synthesized in this study were not fully investigated with changing temperatures. However, Based on the previous work by M. Ge and co-workers [71], the ***B*** sites present in the catalysts were presumably vulnerable to liberate NH_3 (or NH_4^+) species with increasing temperature, resulting in a significant loss in the ***B*** peak intensity at 250 °C (Fig. 13(d)–(f)). In contrast, the ***L*** peaks in the catalysts exhibited strong signals at 250 °C. Therefore, it was highly likely that the Lewis acid sites in the catalysts mainly directed the NH_3-SCR performance upon the adsorption of NH_3 species at low temperatures (*e.g.*, 250 °C), even though the sulfation of the catalysts considerably reduced the quantity of Lewis acid sites (Figs. 7 and 9). Of note, the ***L*** peaks at ~1620 cm^{-1} in the catalysts showed the trend that the peak intensity increased in the following order: Cu_3/DT51 (S) → V_2O_5-WO_3/TiO_2 (S) → Cu_3-$Sb_{1.4}$/DT51 (S). This trend was in close agreement with the results of CO-pulsed chemisorption results showing Cu_3-$Sb_{1.4}$/DT51 (S) had greater quantity of Lewis acid sites than Cu_3/DT51 (S). In addition, this trend was also consistent to that of the NH_3-SCR performance of the catalysts at 220–250 °C, in which greater X_{NOX} and S_{N2} values were observed in the following order: Cu_3/DT51 (S) → V_2O_5-WO_3/TiO_2 (S) → Cu_3-$Sb_{1.4}$/DT51 (S) (Fig. 11).

Of additional note, the NH_3 species adsorbed on the surfaces were rapidly transformed into N_2 and H_2O species after changing the atmosphere from NH_3 to NO/O_2. This was evidenced by the immediate decrease in the intensities of bands featuring NH_3 species chemisorbed onto ***B***/***L*** sites (Fig. 13(g)–(i)). *In situ* DRIFT experiments clarified the surface NH_3-SCR mechanism of the catalysts such that Lewis acid sites were the major surface sites directing the NH_3-SCR performance at low temperatures (*e.g.*, 220–250 °C) and the NH_3-SCR occurred *via* an Eley-Rideal-type reaction between the ***L*** site-adsorbed NH_3 and gaseous NO_X species.

4. Conclusions

In summary, we explored the relationship between NH_3-SCR performance and the copper vanadate crystal structures, which are well-defined in the V_2O_5-CuO binary phase diagram such as CuV_2O_6 (Cu_1), $Cu_2V_2O_7$ (Cu_2), $Cu_3V_2O_8$ (Cu_3), and $Cu_5V_2O_{10}$ (Cu_5). For this investigation, the copper vanadate nanoparticles with sizes of ≤ ~2 nm were dispersed on commercially-available anatase (DT51) to form Cu_X/DT51. Among three copper vanadates with accessible Lewis acid V^{5+} sites (*i.e.*, Cu_2, Cu_3, and Cu_5), Cu_5/DT51 contained the greatest amount of acid sites and showed desired redox behavior at ≤ 250 °C. Thus, Cu_5/DT51 exhibited the greatest NH_3-SCR performance under ideal reaction conditions at low temperatures (*i.e.*, in the presence of NO_X, NH_3, and O_2 balanced by N_2). The inclusion of H_2O and SO_2 into the feed gas stream during NH_3-SCR, however, altered the optimum copper vanadate structure from Cu_5 to Cu_3. This resulted mainly from a substantial increase in the quantity of Brönsted acid sites coupled with improved redox feature of Cu_3/DT51, which were caused by its initial sulfation with SO_2 and O_2 during NH_3-SCR. The Sb promoter content also varied to further improve the NH_3-SCR performance of the optimized sulfated Cu_3/DT51 at low temperatures, where SO_2 or ammonium (bi) sulfates acts as potent surface poison (*i.e.*, < 300 °C). Aside from exhibiting outstanding NH_3-SCR performance over a wide temperature regime (220–400 °C), Cu_3/DT51 with the optimum Sb quantity helped further improve redox feature of Cu_3/DT51 post sulfation. The incorporation of the optimum Sb content into the sulfated Cu_3/DT51 also aided in reducing the surface interactions with SO_2 or ammonium (bi) sulfate, as clarified by the long-term NH_3-SCR experiments at 250 °C. Converting NO_X *via* the Eley-Rideal mechanism, the optimized sulfated Cu_3-$Sb_{1.4}$/DT51 also outperformed the control, a simulated commercial catalyst (V_2O_5-WO_3/TiO_2) for NH_3-SCR. Thus, the optimization of the copper vanadate structure and Sb content of the catalyst was apparently a viable way to promote acid/redox properties and SO_2/ABS resistance for improved NH_3-SCR consequence. Currently, we speculate that sulfation temperature is another major factor that affects the surface properties of copper vanadate catalysts and their NH_3-SCR performance. In addition, it has not been clarified whether there are synergistic effects among Cu and V species in the copper vanadate catalysts. These questions are the subject of on-going investigations in our laboratory.

Contributors

Dr. J. Kim established three key hypotheses for this work and demonstrated these postulations by synthesizing/characterizing the catalysts, testing them in NH_3-SCR under controlled environments, refining the data, and drafting/revising the manuscript. Dr. D. W. Kwon and S. Lee provided partial supports for this work, when performing the experiments and writing the manuscript. Dr. H. P. Ha initially constructed a project associated with this work and provided the comments on the manuscript.

Acknowledgements

We thank Ministry of Science and ICT and National Research Foundation of South Korea for providing a grant for this project (#NRF-2017M3D1A1040690). We also would like to thank Korea Institute of Science and Technology (KIST) for partial support for this project through Future R&D program (#2E28020).

Appendix A. Supplementary data

Supplementary material related to this article can be found, in the online version, at doi:https://doi.org/10.1016/j.apcatb.2018.05.024.

References

[1] I.E. Wachs, Catalysis science of supported vanadium oxide catalysts, Dalton Trans. 42 (2013) 11762–11769.
[2] C.A. Carrero, R. Schloegl, I.E. Wachs, R. Schomaecker, Critical literature review of the kinetics for the oxidative dehydrogenation of propane over well-defined supported vanadium oxide catalysts, ACS Catal. 4 (2014) 3357–3380.
[3] M.O. Guerrero-Pérez, Supported, bulk and bulk-supported vanadium oxide catalysts: a short review with an historical perspective, Catal. Today 285 (2017) 226–233.
[4] M. Ek, Q.M. Ramasse, L. Arnarson, P. Georg Moses, S. Helveg, Visualizing atomic-scale redox dynamics in vanadium oxide-based catalysts, Nat. Commun. 8 (2017) 305.
[5] P. Concepción, H. Knözinger, J.M. López Nieto, A. Martínez-Arias, Characterization of supported vanadium oxide catalysts. Nature of the vanadium species in reduced catalysts, J. Phys. Chem. B 106 (2002) 2574–2582.
[6] B.M. Weckhuysen, D.E. Keller, Chemistry, spectroscopy and the role of supported vanadium oxides in heterogeneous catalysis, Catal. Today 78 (2003) 25–46.
[7] H. Tian, E.I. Ross, I.E. Wachs, Quantitative determination of the speciation of surface vanadium oxides and their catalytic activity, J. Phys. Chem. B 110 (2006) 9593–9600.
[8] M. Hävecker, N. Pinna, K. Weiß, H. Sack-Kongehl, R.E. Jentoft, D. Wang, M. Swoboda, U. Wild, M. Niederberger, J. Urban, D.S. Su, R. Schlögl, Synthesis and functional verification of the unsupported active phase of VxOy catalysts for partial oxidation of n-butane, J. Catal. 236 (2005) 221–232.
[9] I.E. Wachs, B.M. Weckhuysen, Structure and reactivity of surface vanadium oxide species on oxide supports, Appl. Catal. A 157 (1997) 67–90.

[10] E.V. Kondratenko, O. Ovsitser, J. Radnik, M. Schneider, R. Kraehnert, U. Dingerdissen, Influence of reaction conditions on catalyst composition and selective/non-selective reaction pathways of the ODP reaction over V2O3, VO2 and V2O5 with O2 and N2O, Appl. Catal. A 319 (2007) 98–110.
[11] I.E. Wachs, J.-M. Jehng, W. Ueda, Determination of the chemical nature of active surface sites present on bulk mixed metal oxide catalysts, J. Phys. Chem. B 109 (2005) 2275–2284.
[12] T. Feng, J.M. Vohs, TPD–TGA and calorimetric study of the partial oxidation of methanol on TiO2-supported vanadium oxide, J. Catal. 208 (2002) 301–309.
[13] G.S. Wong, M.R. Concepcion, J.M. Vohs, Reactivity of monolayer V2O5 films on TiO2(110) produced via the oxidation of vapor-deposited vanadium, Surf. Sci. 526 (2003) 211–218.
[14] T. Valdés-Solís, G. Marbán, A.B. Fuertes, Kinetics and mechanism of low-temperature SCR of NOx with NH3 over vanadium oxide supported on carbon − ceramic cellular monoliths, Ind. Eng. Chem. Res. 43 (2004) 2349–2355.
[15] B. Guan, R. Zhan, H. Lin, Z. Huang, Review of state of the art technologies of selective catalytic reduction of NOx from diesel engine exhaust, Appl. Therm. Eng. 66 (2014) 395–414.
[16] M. Fu, C. Li, P. Lu, L. Qu, M. Zhang, Y. Zhou, M. Yu, Y. Fang, A review on selective catalytic reduction of NOx by supported catalysts at 100-300 [degree]C-catalysts, mechanism, kinetics, Catal. Sci. Technol. 4 (2014) 14–25.
[17] W. Shan, H. Song, Catalysts for the selective catalytic reduction of NOx with NH3 at low temperature, Catal. Sci. Technol. 5 (2015) 4280–4288.
[18] A. Marberger, D. Ferri, M. Elsener, O. Kröcher, The significance of Lewis acid sites for the selective catalytic reduction of nitric oxide on vanadium-based catalysts, Angew. Chem. Inter. Ed. 55 (2016) 11989–11994.
[19] J.A. Dumesic, N.Y. Topsøe, H. Topsøe, Y. Chen, T. Slabiak, Kinetics of selective catalytic reduction of nitric oxide by ammonia over Vanadia/Titania, J. Catal. 163 (1996) 409–417.
[20] M. Zhu, J.-K. Lai, U. Tumuluri, M.E. Ford, Z. Wu, I.E. Wachs, Reaction pathways and kinetics for selective catalytic reduction (SCR) of acidic NOx Emissions from power plants with NH3, ACS Catal. 7 (2017) 8358–8361.
[21] N.-Y. Topsøe, Mechanism of the selective catalytic reduction of nitric oxide by ammonia elucidated by in situ on-line fourier transform infrared spectroscopy, Science 265 (1994) 1217–1219.
[22] H. Kamata, K. Takahashi, C.U. Ingemar Odenbrand, Kinetics of the selective reduction of NO with NH3 over a V2O5(WO3)/TiO2 commercial SCR catalyst, J. Catal. 185 (1999) 106–113.
[23] G. Busca, L. Lietti, G. Ramis, F. Berti, Chemical and mechanistic aspects of the selective catalytic reduction of NOx by ammonia over oxide catalysts: a review, Appl. Catal. B 18 (1998) 1–36.
[24] C. Wang, S. Yang, H. Chang, Y. Peng, J. Li, Dispersion of tungsten oxide on SCR performance of V2O5WO3/TiO2: acidity, surface species and catalytic activity, Chem. Eng. J. 225 (2013) 520–527.
[25] I. Song, S. Youn, H. Lee, S.G. Lee, S.J. Cho, D.H. Kim, Effects of microporous TiO2 support on the catalytic and structural properties of V2O5/microporous TiO2 for the selective catalytic reduction of NO by NH3, Appl. Catal. B 210 (2017) 421–431.
[26] K. Skalska, J.S. Miller, S. Ledakowicz, Trends in NOx abatement: a review, Sci. Total Environ. 408 (2010) 3976–3989.
[27] U. Diebold, The surface science of titanium dioxide, Surf. Sci. Rep. 48 (2003) 53–229.
[28] S. Gillot, G. Tricot, H. Vezin, J.-P. Dacquin, C. Dujardin, P. Granger, Development of stable and efficient CeVO4 systems for the selective reduction of NOx by ammonia: structure-activity relationship, Appl. Catal. B 218 (2017) 338–348.
[29] X. Zhao, L. Huang, H. Li, H. Hu, X. Hu, L. Shi, D. Zhang, Promotional effects of zirconium doped CeVO4 for the low-temperature selective catalytic reduction of NOx with NH3, Appl. Catal. B 183 (2016) 269–281.
[30] F. Liu, H. He, Z. Lian, W. Shan, L. Xie, K. Asakura, W. Yang, H. Deng, Highly dispersed iron vanadate catalyst supported on TiO2 for the selective catalytic reduction of NOx with NH3, J. Catal. 307 (2013) 340–351.
[31] A. Marberger, M. Elsener, D. Ferri, A. Sagar, K. Schermanz, O. Kröcher, Generation of NH3 selective catalytic reduction active catalysts from decomposition of supported FeVO4, ACS Catal. 5 (2015) 4180–4188.
[32] X. Zhao, L. Huang, H. Li, H. Hu, J. Han, L. Shi, D. Zhang, Highly dispersed V2O5/TiO2 modified with transition metals (Cu, Fe, Mn, Co) as efficient catalysts for the selective reduction of NO with NH3, Chin. J. Catal. 36 (2015) 1886–1899.
[33] T. Kawada, S. Hinokuma, M. Machida, Structure and SO3 decomposition activity of nCuO–V2O5/SiO2 (n = 0, 1, 2, 3 and 5) catalysts for solar thermochemical water splitting cycles, Catal. Today 242 (2015) 268–273.
[34] T. Kawada, T. Tajiri, H. Yamashita, M. Machida, Molten copper hexaoxodivanadate: an efficient catalyst for SO3 decomposition in solar thermochemical water splitting cycles, Catal. Sci. Technol. 4 (2014) 780–785.
[35] Y. Feng, X. Li, Z. Shao, H. Wang, Morphology-dependent performance of Zn2GeO4 as a high-performance anode material for rechargeable lithium ion batteries, J. Mater. Chem. A 3 (2015) 15274–15279.
[36] M. Machida, T. Kawada, S. Hebishima, S. Hinokuma, S. Takeshima, Macroporous supported Cu–V oxide as a promising substitute of the Pt catalyst for sulfuric acid decomposition in solar thermochemical hydrogen production, Chem. Mater. 24 (2012) 557–561.
[37] L. Muzio, S. Bogseth, R. Himes, Y.-C. Chien, D. Dunn-Rankin, Ammonium bisulfate formation and reduced load SCR operation, Fuel 206 (2017) 180–189.
[38] C. Li, M. Shen, T. Yu, J. Wang, J. Wang, Y. Zhai, The mechanism of ammonium bisulfate formation and decomposition over V/WTi catalysts for NH3-selective catalytic reduction at various temperatures, Phys. Chem. Chem. Phys. 19 (2017) 15194–15206.
[39] H.H. Phil, M.P. Reddy, P.A. Kumar, L.K. Ju, J.S. Hyo, SO2 resistant antimony promoted V2O5/TiO2 catalyst for NH3-SCR of NOx at low temperatures, Appl. Catal. B 78 (2008) 301–308.
[40] B. Thirupathi, P.G. Smirniotis, Nickel-doped Mn/TiO2 as an efficient catalyst for the low-temperature SCR of NO with NH3: catalytic evaluation and characterizations, J. Catal. 288 (2012) 74–83.
[41] K.J. Lee, P.A. Kumar, M.S. Maqbool, K.N. Rao, K.H. Song, H.P. Ha, Ceria added Sb-V2O5/TiO2 catalysts for low temperature NH3 SCR: physico-chemical properties and catalytic activity, Appl. Catal. B 142-143 (2013) 705–717.
[42] D.W. Kwon, K.B. Nam, S.C. Hong, The role of ceria on the activity and SO2 resistance of catalysts for the selective catalytic reduction of NOx by NH3, Appl. Catal. B 166-167 (2015) 37–44.
[43] M.S. Maqbool, A.K. Pullur, H.P. Ha, Novel sulfation effect on low-temperature activity enhancement of CeO2-added Sb-V2O5/TiO2 catalyst for NH3-SCR, Appl. Catal. B 152-153 (2014) 28–37.
[44] D.W. Kwon, S. Chang Hong, Enhancement of performance and sulfur resistance of ceria-doped V/Sb/Ti by sulfation for selective catalytic reduction of NOx with ammonia, RSC Adv. 6 (2016) 1169–1181.
[45] J. Kim, M.S. Abbott, D.B. Go, J.C. Hicks, Enhancing C–H bond activation of methane via temperature-controlled, catalyst–plasma interactions, ACS Energy Lett. 1 (2016) 94–99.
[46] D.J. Rensel, J. Kim, V. Jain, Y. Bonita, N. Rai, J.C. Hicks, Composition-directed FeXMo2-XP bimetallic catalysts for hydrodeoxygenation reactions, Catal. Sci. Technol. 7 (2017) 1857–1867.
[47] J. Kim, D.B. Go, J.C. Hicks, Synergistic effects of plasma-catalyst interactions for CH4 activation, Phys. Chem. Chem. Phys. 19 (2017) 13010–13021.
[48] P. Mehta, P. Barboun, F.A. Herrera, J. Kim, P. Rumbach, D.B. Go, J.C. Hicks, W.F. Schneider, Overcoming ammonia synthesis scaling relations with plasma-enabled catalysis, Nat. Catal. 1 (2018) 269–275.
[49] Y.J. Choe, J.Y. Byun, S.H. Kim, J. Kim, Fe3S4/Fe7S8-promoted degradation of phenol via heterogeneous, catalytic H2O2 scission mediated by S-modified surface Fe2 + + species, Appl. Catal. B 233 (2018) 272–280.
[50] M. Inomata, K. Mori, A. Miyamoto, T. Ui, Y. Murakami, Structures of supported vanadium oxide catalysts. 1. Vanadium(V) oxide/titanium dioxide (anatase), vanadium(V) oxide/titanium dioxide (rutile), and vanadium(V) oxide/titanium dioxide (mixture of anatase with rutile), J. Phys. Chem. 87 (1983) 754–761.
[51] Z. Liu, S. Ihl Woo, Recent advances in catalytic DeNOX science and technology, Cat. Rev. 48 (2006) 43–89.
[52] Y. Yu, J. Miao, J. Wang, C. He, J. Chen, Facile synthesis of CuSO4/TiO2 catalysts with superior activity and SO2 tolerance for NH3-SCR: physicochemical properties and reaction mechanism, Catal. Sci. Technol. 7 (2017) 1590–1601.
[53] M. Li, Y. Gao, N. Chen, X. Meng, C. Wang, Y. Zhang, D. Zhang, Y. Wei, F. Du, G. Chen, Cu3V2O8 nanoparticles as intercalation-type anode material for lithium-ion batteries, Chem. Eur. J. 22 (2016) 11405–11412.
[54] D.W. Kwon, K.B. Nam, S.C. Hong, Influence of tungsten on the activity of a Mn/Ce/W/Ti catalyst for the selective catalytic reduction of NO with NH3 at low temperatures, Appl. Catal. A 497 (2015) 160–166.
[55] W. Shan, F. Liu, H. He, X. Shi, C. Zhang, The remarkable improvement of a Ce—Ti based catalyst for NOx abatement, prepared by a homogeneous precipitation method, ChemCatChem 3 (2011) 1286–1289.
[56] F. Lónyi, J. Valyon, On the interpretation of the NH3-TPD patterns of H-ZSM-5 and H-mordenite, Micro. Meso. Mater. 47 (2001) 293–301.
[57] F. Hemmann, C. Jaeger, E. Kemnitz, Comparison of acidic site quantification methods for a series of nanoscopic aluminum hydroxide fluorides, RSC Adv. 4 (2014) 56900–56909.
[58] G. Ramis, L. Yi, G. Busca, M. Turco, E. Kotur, R.J. Willey, Adsorption, activation, and oxidation of ammonia over SCR catalysts, J. Catal. 157 (1995) 523–535.
[59] L. Chmielarz, A. Węgrzyn, M. Wojciechowska, S. Witkowski, M. Michalik, Selective catalytic oxidation (SCO) of ammonia to nitrogen over hydrotalcite originated Mg–Cu–Fe mixed metal oxides, Catal. Lett. 141 (2011) 1345–1354.
[60] J.-M. Jehng, G. Deo, B.M. Weckhuysen, I.E. Wachs, Effect of water vapor on the molecular structures of supported vanadium oxide catalysts at elevated temperatures, J. Mol. Catal. A 110 (1996) 41–54.
[61] M. Turco, L. Lisi, R. Pirone, P. Ciambelli, Effect of water on the kinetics of nitric oxide reduction over a high-surface-area V2O5/TiO2 catalyst, Appl. Catal. B 3 (1994) 133–149.
[62] S. Yang, Y. Guo, H. Chang, L. Ma, Y. Peng, Z. Qu, N. Yan, C. Wang, J. Li, Novel effect of SO2 on the SCR reaction over CeO2: mechanism and significance, Appl. Catal. B 136-137 (2013) 19–28.
[63] W. Jing, Q. Guo, Y. Hou, G. Ma, X. Han, Z. Huang, Catalytic role of vanadium(V) sulfate on activated carbon for SO2 oxidation and NH3-SCR of NO at low temperatures, Catal. Commun. 56 (2014) 23–26.
[64] C. Yanxin, J. Yi, L. Wenzhao, J. Rongchao, T. Shaozhen, H. Wenbin, Adsorption and interaction of H2S/SO2 on TiO2, Catal. Today 50 (1999) 39–47.
[65] W. Xu, H. He, Y. Yu, Deactivation of a Ce/TiO2 catalyst by SO2 in the selective catalytic reduction of NO by NH3, J. Phys. Chem. C 113 (2009) 4426–4432.
[66] D.W. Kwon, K.H. Park, S.C. Hong, Enhancement of SCR activity and SO2 resistance on VOx/TiO2 catalyst by addition of molybdenum, Chem. Eng. J. 284 (2016) 315–324.
[67] S.M. Lee, K.H. Park, S.C. Hong, MnOx/CeO2–TiO2 mixed oxide catalysts for the selective catalytic reduction of NO with NH3 at low temperature, Chem. Eng. J. 195-196 (2012) 323–331.
[68] W. Shan, F. Liu, H. He, X. Shi, C. Zhang, A superior Ce-W-Ti mixed oxide catalyst for the selective catalytic reduction of NOx with NH3, Appl. Catal. B 115-116 (2012) 100–106.
[69] G. Qi, R.T. Yang, Performance and kinetics study for low-temperature SCR of NO with NH3 over MnOx–CeO2 catalyst, J. Catal. 217 (2003) 434–441.

[70] N.Y. Topsoe, J.A. Dumesic, H. Topsoe, Vanadia-Titania catalysts for selective catalytic reduction of nitric-oxide by ammonia: I.I. Studies of active sites and formulation of catalytic cycles, J. Catal. 151 (1995) 241–252.
[71] L. Chen, J. Li, M. Ge, DRIFT study on cerium − tungsten/titiania catalyst for selective catalytic reduction of NOx with NH3, Environ. Sci. Technol. 44 (2010) 9590–9596.
[72] S.D. Lin, A.C. Gluhoi, B.E. Nieuwenhuys, Ammonia oxidation over Au/MOx/γ-Al2O3—activity, selectivity and FTIR measurements, Catal. Today 90 (2004) 3–14.
[73] M.A. Larrubia, G. Ramis, G. Busca, An FT-IR study of the adsorption of urea and ammonia over V2O5–MoO3–TiO2 SCR catalysts, Appl. Catal. B 27 (2000) L145-L1.